Journal of Advanced Ceramics
2016, **5**(3): 253–261
DOI: 10.1007/s40145-016-0197-x

ISSN 2226-4108
CN 10-1154/TQ

Research Article

Investigation on the laser ablation of SiC ceramics using micro-Raman mapping technique

Chaoli FU[a,b], Yong YANG[a,*], Zhengren HUANG[a,*], Guiling LIU[a], Hui ZHANG[a], Fang JIANG[a], Yuquan WEI[a], Zheng JIAO[b]

[a]*Structural Ceramic Engineering Research Center, Shanghai Institute of Ceramics, Chinese Academy of Sciences, 1295 Dingxi Road, Shanghai 200050, China*
[b]*College of Environmental and Chemical Engineering, Shanghai University, 99 Shangda Road, Shanghai 200444, China*

Received: April 13, 2016; Revised: May 25, 2016; Accepted: June 14, 2016

Abstract: Research on the laser ablation behavior of SiC ceramics has great significance for the improvement of their anti-laser ability as high-performance mirrors in space and lasers, or the laser surface micro-machining technology as electronic components in micro-electron mechanical systems (MEMS). In this work, the laser ablation of SiC ceramics has been performed by using laser pulses of 12 ns duration at 1064 nm. The laser induced damage threshold (LIDT) below 0.1 J/cm^2 was obtained by 1-on-1 mode and its damage morphology appeared in the form of "burning crater" with a clear boundary. Micro-Raman mapping technique was first introduced in our study on the laser ablation mechanisms of SiC surface by identifying physical and chemical changes between uninjured and laser-ablated areas. It has been concluded that during the ablation process, SiC surface mainly underwent decomposition to the elemental Si and C, accompanied by some transformation of crystal orientation. The oxidation of SiC also took place but only in small amount on the edges of target region, while there was no hint of SiO_2 in the center with higher energy density, maybe because of deficiency of O_2 atmosphere in the ablated area, elimination of SiO_2 by carbon at 1505 ℃, or evaporating at 2230 ℃.

Keywords: silicon carbide (SiC); laser ablation; micro-Raman mapping technique; decomposition; oxidation

1 Introduction

Compared to traditional mirror materials including the first generation glass-ceramic and the second one mainly made of beryllium metal and its alloys, silicon carbide (SiC) as the third generation mirror material gets a lot of outstanding properties such as high-temperature capability, moderate strength, good wear resistance, and high thermal conductivity. SiC ceramics have gradually been identified as the most promising material for optical mirrors in large-scale space optical devices and high-power laser systems [1,2]. As such high-performance optical mirror, it must possess stable and high-quality surface to resist deformation and damage from laser attack. In addition, SiC has wider band gap, higher breakdown field, and higher saturation velocity than silicon, recognized as the most potential electronic component for micro-electron

* Corresponding authors.
E-mail: Y. Yang, yangyong@mail.sic.ac.cn;
Z. Huang, zhrhuang@mail.sic.ac.cn

mechanical systems (MEMS) [3–5] used in harsh environment. Instead of the difficulty in conventional mechanical machining on the surface of SiC elements due to their extreme thermodynamic stability and chemical inertness, pulse laser ablation is emerging as an attractive alternative, offering a clean and simple method with high etch rate [6–8]. Therefore, knowledge of the laser ablation process of SiC ceramics can be necessary and meaningful.

Most investigations about laser ablation behavior of SiC surface have been carried out with focus on the dependencies among ablation fluence, rate, and topography [8–10]. There are also some reports involving the changes of chemical composition after laser irradiation that Si and O elements are both detected by surface analytical techniques such as energy dispersive spectrometer (EDS), X-ray photoelectron spectroscopy (XPS), Auger electron spectroscopy (AES), or Raman, confirming the oxidation and decomposition of SiC [11,12]. However, there was no comprehensive comparison of composition distributions between uninjured and laser-ablated areas on the SiC surface, which can help elaborate chemical reactions and laser ablation mechanisms more clearly. Therefore, further work is required to explore the interaction process between laser and SiC ceramics by characterizing the distribution of chemical components and structures.

Micro-Raman spectroscopy (μ-RS) is a kind of nondestructive and relatively fast surface characterization technique to identify the chemical components and structures, with high spatial resolution and no need for special treatment of samples [13,14]. SiC ceramics have several kinds of crystal forms, and could be easily detected and distinguished in Raman spectra that provide a wide range of information about the chemical structures with very strong signal of frequency, intensity, and width [15–17], so that μ-RS has been used in detecting the composition changes of laser-ablated SiC surface [11,12]. Moreover, micro-Raman mapping technology, a spatially resolved technique, allows one to characterize the phase distribution of chemical structures in a specific region of material surface by 2D images [18–20], possibly an effective technique to study the laser ablation of SiC ceramics.

Accordingly, micro-Raman mapping technique was first introduced in our study. With this technique, physical and chemical changes on the SiC surface were identified point to point, so that the chemical reactions were inferred and the laser ablation process was accordingly explored. Here the laser induced damage threshold (LIDT) of SiC was determined in 1-on-1 mode. Atomic force microscope (AFM) and scanning electron microscopy (SEM) were used to characterize the morphology of unprocessed and ablated surfaces.

2 Experimental details

2. 1 Preparation of SiC samples

The pressureless solid-phase sintering ceramics (S-SiC) with a volume density of 3.136 g/cm^3 were polished to obtain optical surface with roughness of 2 nm RMS (root mean square, in 10 μm × 10 μm area). Phase analysis of S-SiC ceramics was performed by X-ray diffraction (XRD, D/max2500V) in Fig. 1. It is shown that the SiC sample contains multi-crystal structures including main phase α-SiC (6H-SiC and 4H-SiC) and a little residual carbon C attributed to the use of C black as a sintering aid.

Figure 2 shows the optical microscopy image of the SiC surface. The gray part is of main phase SiC, and black dots scattered on the surface can be attributed to the residual carbon C or some voids, already demonstrated by Chen *et al*. [21].

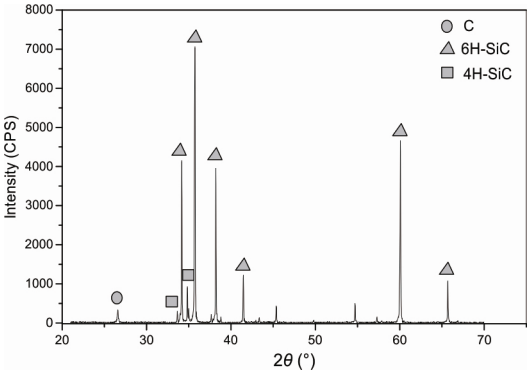

Fig. 1 XRD pattern of the S-SiC ceramic.

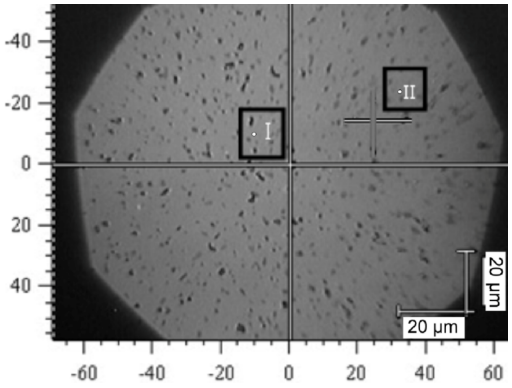

Fig. 2 Optical microscopy image of SiC surface.

2. 2 Test of LIDT and morphology observation

The laser induced damage threshold (LIDT) is defined as the lowest laser fluence at which a permanent change occurs in the optical material as a result of laser illumination [22]. That change is typically observed by image difference method or plasma spark method. In our study, the LIDT of the polished SiC ceramic at 1064 nm was evaluated under 1-on-1 test mode according to the standard ISO11254-1 [23] by plotting the damage frequency in dependence on the pulse fluence and extrapolating the damage frequency to zero. Laser damage test apparatus and the operation principle in this study are described in the literature [24]. In the experiment, the pulses of $\tau = 12$ ns were focused at normal beam incident angle on the sample yielding a Gaussian beam spot with an effective area of 0.12 mm^2. During testing, the pulse energy density of laser was adjusted by gradually decreasing from 7 J/cm^2 and the repetition rate was 5 Hz.

The surface topographic signatures of SiC substrate were characterized in detail by the atomic force microscope (AFM, SPI3800N&SPA300HV) in ambient atmosphere at room temperature in contact mode. The morphology of ablated cavity and its surroundings was observed by a scanning electron microscope (SEM, Model JSM-6700F and S-4800).

2. 3 Surface characterization by micro-Raman mapping technique

In this work, a Renishaw inVia micro-Raman spectrometer system [25] was used to analyze the Raman spectra of SiC surface. This device comprises of a focused and stable laser with the wavelength of 514 nm to generate the power of 1–2 mW, an optical microscope having the 100× objective lens, and a high-resolution monochromator. During the measurement, the incident and scattered beams were focused to the sample, producing a laser spot with diameter of ~1 μm and high resolution of 1 μm in lateral direction and 1.7 μm in vertical direction. At the beginning of the experiment, the single Raman spectra for two spots I and II on the SiC surface (see Fig. 2) were collected with the average collection time of 10 s for each spectrum, so as to determine the components on the uninjured and laser-ablated surfaces of SiC.

To produce 2D maps of component and structure distributions on the surface, micro-Raman mapping technique was performed on the defined area ranging along both X and Y axes from −350 to +350 μm. The details are described as follows [26,27]. The SiC ceramic was placed in a two-dimensional automatic control platform, and a piezo stage was used to move the sample with a step size of 20.8 μm so that the Raman spectrum at every point was collected for about 30 s. All those Raman spectra were auto-matched to the standard of a certain component detected by the single Raman spectrum (including the peak position, relative peak intensity, and full width at half maximum (FWHM)) by using the Renishaw WIRE software with a mixed Lorentzian and Gaussian peak fitting function, and 2D Raman images were constructed.

3 Results

3. 1 LIDT and ablation morphology

LIDT of the SiC sample at 1064 nm was investigated under the 1-on-1 mode and the fitting result is shown in Fig. 3. It can be seen that the LIDT of polished SiC surface by nanosecond laser is very low, ~0.1 J/cm^2, below which the damage probability is 100%.

SEM analysis has been performed on the damaged site of SiC to better infer the ablation features. Figure 4 shows the SEM image of the laser-ablated surface of SiC sample relative to an incident fluence $F = 0.2$ J/cm^2. As one can note, the ablation morphology appears in the form of a burning crater with a clear boundary between damaged area and uninjured area. There are neither obvious cracks nor melt damages in the surrounding areas caused by thermal stress and heat transmission. Furthermore, the widest gap of the ablation region is about 300 μm within the range of laser beam radiation. Therefore, the ablation region can be defined by controlling the laser spot size and the fluence.

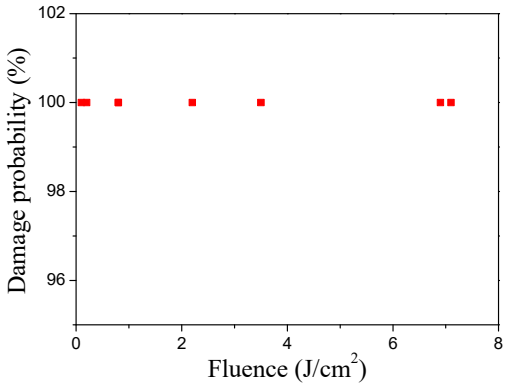

Fig. 3 LIDT result of the SiC surface ($\lambda = 1064$ nm, $\tau = 12$ ns).

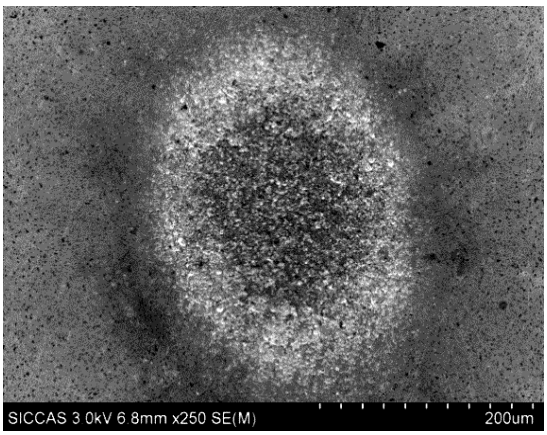

Fig. 4 SEM morphology of laser-ablated SiC surface at $F = 0.2$ J/cm^2.

In addition, it seems that the edges of the ablated region are covered with re-solidified melt phases while the center presents a deeper and stronger burning pit where some materials seem to be removed, maybe induced by uneven beam energy and temperature distribution of Gaussian beam to accumulate higher energy density to the center area than that on the edges.

3. 2 Chemical composition properties

3. 2. 1 Uninjured surface of SiC

The μ-RS results of uninjured area on SiC are depicted in Fig. 5. Spectra Fig. 5(a) derives from the point I and Fig. 5(b) from the point II. The sharp peaks in the region of 750–800 cm^{-1} (at 767, 788, and 796 cm^{-1}) represent the transversal optical modes and that at 964 cm^{-1} the longitudinal optical modes of the polycrystalline SiC [28]. Also the bands of the graphite are detectable as D-peak at 1359 cm^{-1} and the G-peak at 1591 cm^{-1} [29]. These results are in agreement with those shown in the XRD pattern.

The intensity distribution maps of those characterized bands at 1359, 1591, 788, and 964 cm^{-1} are shown in Fig. 6. From the distribution images of peaks 788 cm^{-1} (Fig. 6(a)) and 964 cm^{-1} (Fig. 6(b)), it can be observed that the phase SiC is continuously distributed on the surface. Similarly, as shown in the distribution images of peaks 1359 cm^{-1} (Fig. 6(c)) and 1591 cm^{-1} (Fig. 6(d)), the phase C is uniformly scattered in the phase SiC.

3. 2. 2 Laser-ablated surface of SiC

The μ-RS results of laser-ablated area on SiC are depicted in Fig. 7. Spectra Fig. 7(a) derives from the point I and Fig. 7(b) from the point II. Besides those

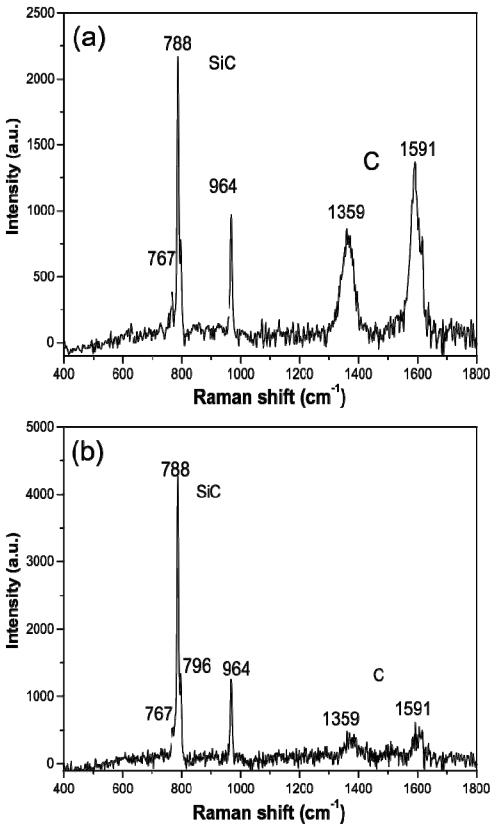

Fig. 5 Raman spectra of untreated SiC surface at points (a) I and (b) II.

characterized bands of α-SiC (at 796, 767, 788, and 964 cm^{-1}) and those characterized bands of C (at 1359 and 1591 cm^{-1}), a new band at ~521 cm^{-1} appears and can be attributed to the crystalline silicon [11,30]. Obviously, the Si component of SiC undergoes reduction to the elemental state. Besides, bands at 1359 and 1591 cm^{-1} attributed to carbon become overlapped to some extent and the full width at half maximum (FWHM) gets a bit wider than that before laser treatment, maybe because of the appearance of new crystal phase for carbon, as Yi *et al*. [31] have reported that some SiC are decomposed after electron beam evaporation and generates a quantity of diamond-like carbon phase. It can be concluded that the laser irradiation has caused the decomposition of SiC, generating the elemental Si and C. Furthermore, it can also be observed that after laser treatment, the Raman intensity of the band at 964 cm^{-1} respect to 788 cm^{-1} becomes enhanced, indicating the transformation of crystal orientation.

The intensity distribution maps of those characterized bands at 521, 1359, 1591, 788, and 964 cm^{-1} are shown in Fig. 8. In the laser-irradiated area, only a small amount of α-SiC still remains as shown in Figs. 8(b) and

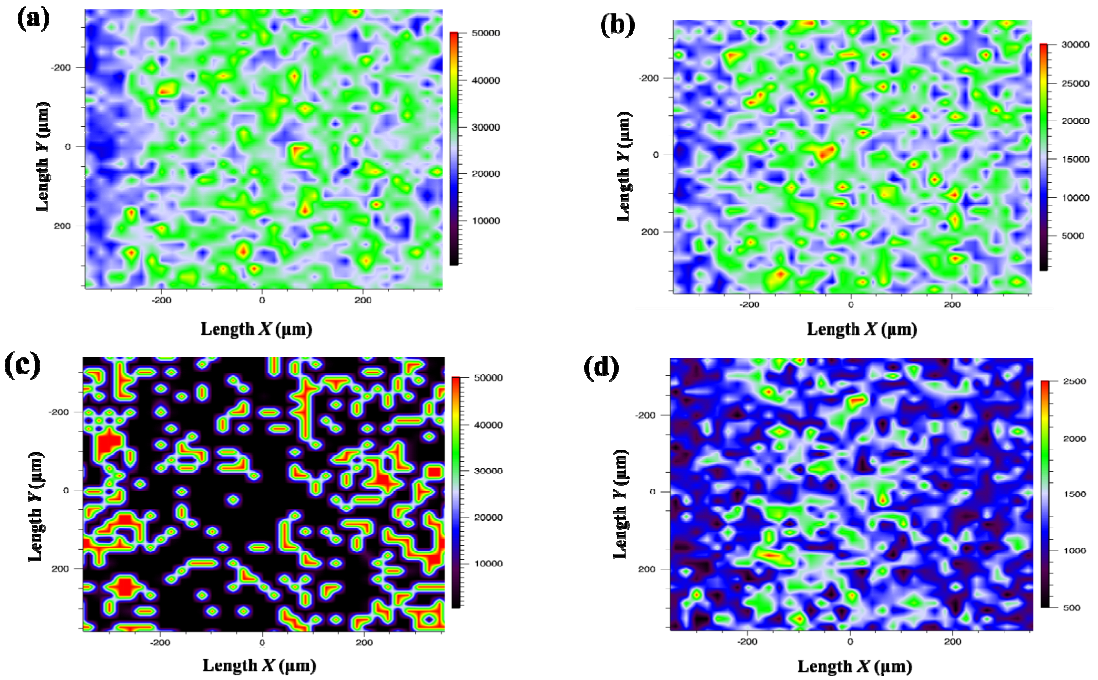

Fig. 6 Raman maps of untreated SiC surface based on the intensity distribution of characterized bands at (a) 788 cm^{-1}, (b) 964 cm^{-1}, (c) 1359 cm^{-1}, and (d) 1591 cm^{-1}. Right-hand scale represents the relative band intensity.

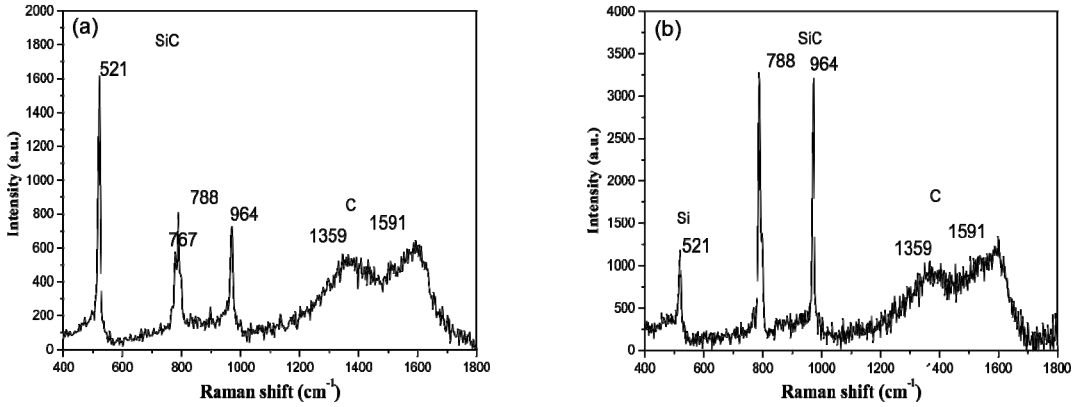

Fig. 7 Raman spectra of laser-ablated SiC surface at points (a) I and (b) II.

8(c); however, large quantity of Si (Fig. 8(a)) and quite a part of continuous C (Figs. 8(d) and 8(e)) different from the intrinsic C scattered in untreated area are observed, indicating the decomposition of SiC. In other position without laser irradiation, no phase Si can be seen, but only the phase C is evenly distributed in the continuous SiC matrix.

4 Discussion

4. 1 Laser absorption mechanism of SiC surface

The laser ablation on the SiC surface can be mostly ascribed to an excess of thermal energy which is coupled into the material by high laser absorption. The laser absorption mechanisms of polycrystalline silicon carbide ceramics are complicated.

The semiconductor silicon carbide (SiC) has a direct band gap of $E_g = 3.08$ eV. Since the liner absorption of the laser with the wavelength of $\lambda = 200$ nm ($E_{photon} = 4.7$ eV) and the two-photon absorption of the laser with the wavelength of $\lambda = 800$ nm ($E_{photon} = 1.6$ eV) to cross the band gap of SiC have been discussed in some reports [11], three photons of the energy $E_{photon} = 1.17$ eV for 1064 nm wavelength laser are sufficient to cross the band gap. Therefore, the multi-photon absorption mechanism here is quite possible during the interaction between pulse laser and SiC ceramics [9]. A

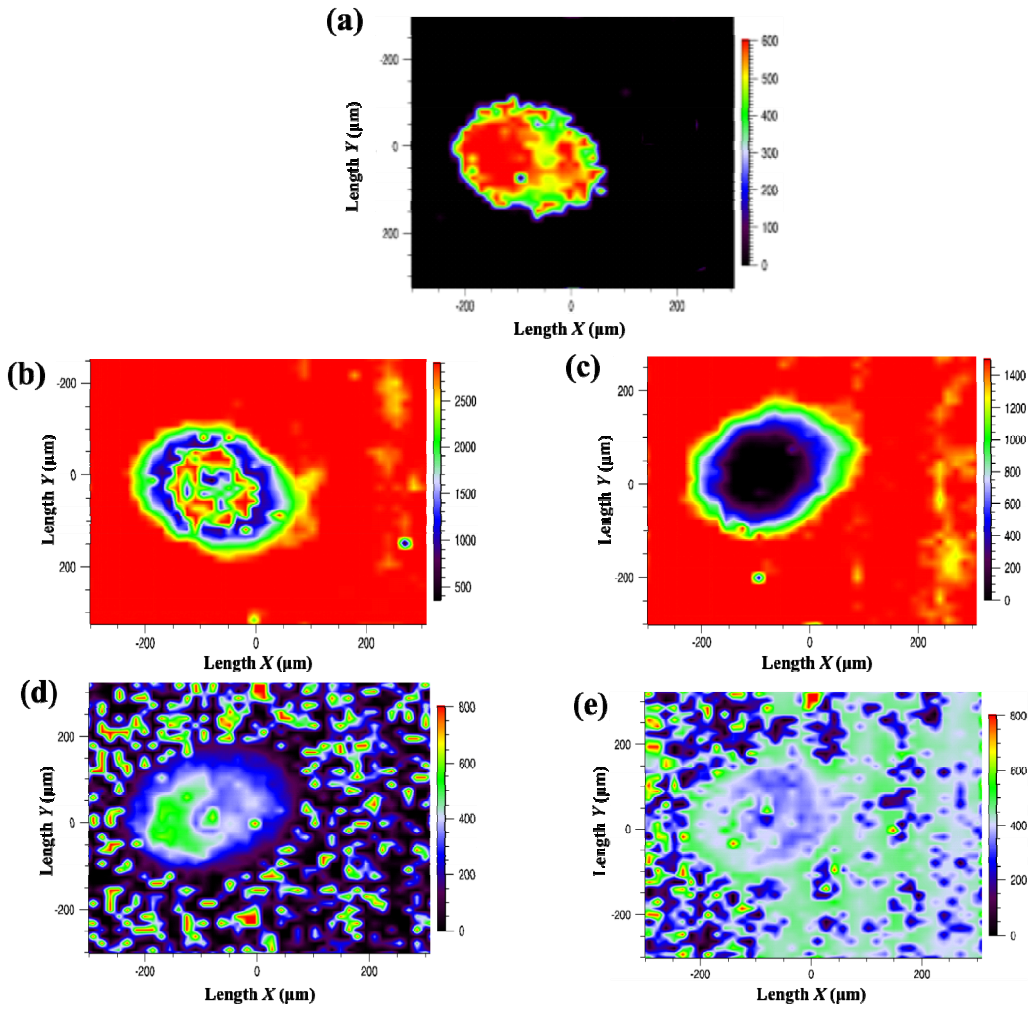

Fig. 8 Raman maps of laser-ablated SiC surface based on the intensity distribution of characterized bands at (a) 521 cm^{-1}, (b) 788 cm^{-1}, (c) 964 cm^{-1}, (d) 1359 cm^{-1}, and (e) 1591 cm^{-1}. Right-hand scale represents the relative band intensity.

few of laser photons are absorbed by SiC in the way of electronic transition from the forbidden band to the conduction band. Free carriers in conduction band are easily excited to a higher energy state by the photoelectric field acceleration, resulting in avalanche ionization and rapidly accumulating the energy to the ablated region.

As we all know, the surface of SiC tends to get intrinsic impurities and defects during its preparation and processing, and adsorbs ambient contaminants during its storage and transportation. Figure 9 shows the AFM topography of polished SiC surface where some bright bumps, dark pits, and scratches are observed. The bumps are contaminants, the second phase C, or SiC grains staying on the surface after grinding. And the pits are from the exposure of internal pore or the grain stripping out of the matrix during the optical structuring. All those defects change the temperature field and the electron field, promoting the absorption and gathering of laser energy to the ablated area. In addition, the internal structures of the polycrystalline silicon carbide ceramics comprise of grain boundaries and pores [32], which cause laser photon scattering and gathering to the ablated region. Therefore, we should take measures to optimize the preparation process and surface modification of the SiC ceramics to obtain high density, less lattice defects, and good-quality surface for low laser absorption, low scattering, and high LIDT when used as special optical mirrors.

4. 2 Laser ablation mechanism of SiC surface

As depicted in the laser ablation morphology of SiC surface (see Fig. 4), there is no obvious cracking or delamination but rather the melt crater, indicating that the surface material reaches its critical stage for thermal damage prior to the threshold of stress cracking. It is

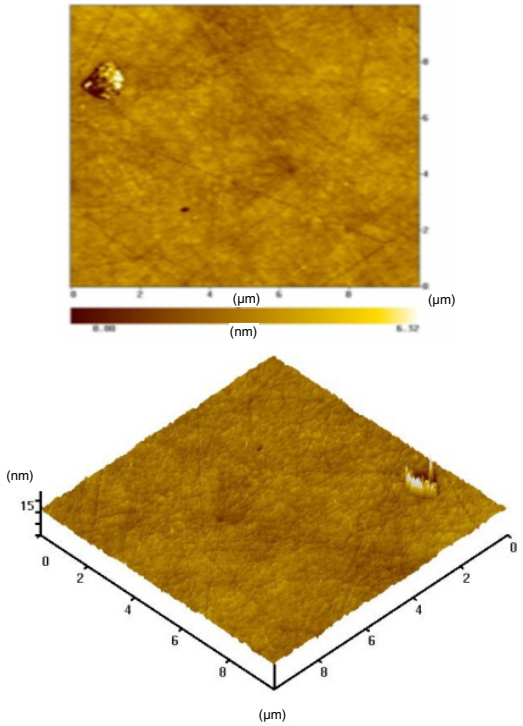

Fig. 9 AFM images of polished SiC surface within 10 μm × 10 μm area.

evidenced from the ablation profile that the nanosecond laser causes destruction only within the irradiated area and does no influence on surrounding material by heat transmission. Such characteristics may be ascribed to the presence of grain boundaries and lattice defects that restrict the effective transmission of absorbed photon energy to other areas without laser irradiation [33] in the short time of interaction between nanosecond laser and the material. Therefore, the ablated region can be defined by controlling the laser spot size and the fluence, which offers a possibility of surface micro-processing with short-pulse laser on the SiC ceramics efficiently and accurately.

Chemical changes shown in 2D images of Raman indicate the decomposition of SiC to new phases Si and C by laser energy accumulation, equivalent to its thermal decomposition at the temperature of above 2300 ℃. Also it is demonstrated that the ablation process was simultaneously accompanied by some transformation of crystal orientation (see the Raman spectra of SiC ceramic), re-solidification, and the removal of materials by evaporating.

There are some reports [11,12,34] that the α-SiC is mainly oxidized as shown in the chemical equations (1)–(3), producing SiO_2 and gaseous carbon dioxides (such as CO, CO_2, and CH_4, etc.) after laser irradiation. According to thermodynamic expectations, SiO_2 or even silicon oxycarbides (SiC_xO_y) can grow from the oxidation of α-SiC in the atmosphere containing oxygen around 1200 ℃ [35,36], which could happen much more easily than its thermal decomposition based on the consideration of the reaction temperature. However in our work, the case has some changes with the thermodynamic behavior and reported results. Figure 10 shows the element composition of SiC surface by electron microprobe. We can note that O element appears occasionally and in small amount on the edges of ablated region (see Fig. 10(d) for the area 4). In the areas 1, 2, and 3, only Si and C elements are detected and remained almost the same Si/C ratio in spite of the laser irradiation as shown in Table 1. Generally, the ratio of Si/C could not change in the process of SiC decomposition into Si and C, while the ratio would change obviously in the process of SiC oxidation. These EDS results provide the information that the oxidation of SiC has taken place but only in small amounts on the edges of laser irradiation. As we all know, the Gaussian laser beam induces uneven energy and temperature distribution between the center area and the edges of the target, which may affect the chemical changes. In the center of ablated area with high laser energy density, there is no hint of SiO_2 from the oxygen of SiC, maybe because of several following reasons. First of all, during the nanosecond laser irradiation, there might not be enough time for O_2 and water vapor to diffuse efficiently to the irradiated spots, resulting in that the oxidation would only take place in very small area. Secondly, the generated SiO_2 is possibly eliminated by C at 1505 ℃ as Eq. (4) [21]. Furthermore, besides gaseous carbon dioxides, the generated SiO_2 can also be evaporating at 2230 ℃ (below the decomposition temperature of SiC ceramics). Thus all the evaporation results in material removal to leave the crater. However, on the edges of ablated region with lower accumulated laser energy, SiO_2 could be produced and re-solidified on the surface.

$$SiC + 3/2O_2 \rightarrow SiO_2 + CO \quad (1)$$

$$SiC + 2O_2 \rightarrow SiO_2 + CO_2 \quad (2)$$

$$SiC + 2H_2O \rightarrow SiO_2 + CH_4 \quad (3)$$

$$SiO_2 + 2C \rightarrow SiC + 2CO \quad (4)$$

Table 1 Si/C content ratio of different regions on SiC surface

Element	C	Si	O
Area 1	35.47	64.53	—
Area 2	34.80	65.20	—
Area 3	35.20	64.80	—
Area 4	34.40	60.00	5.60

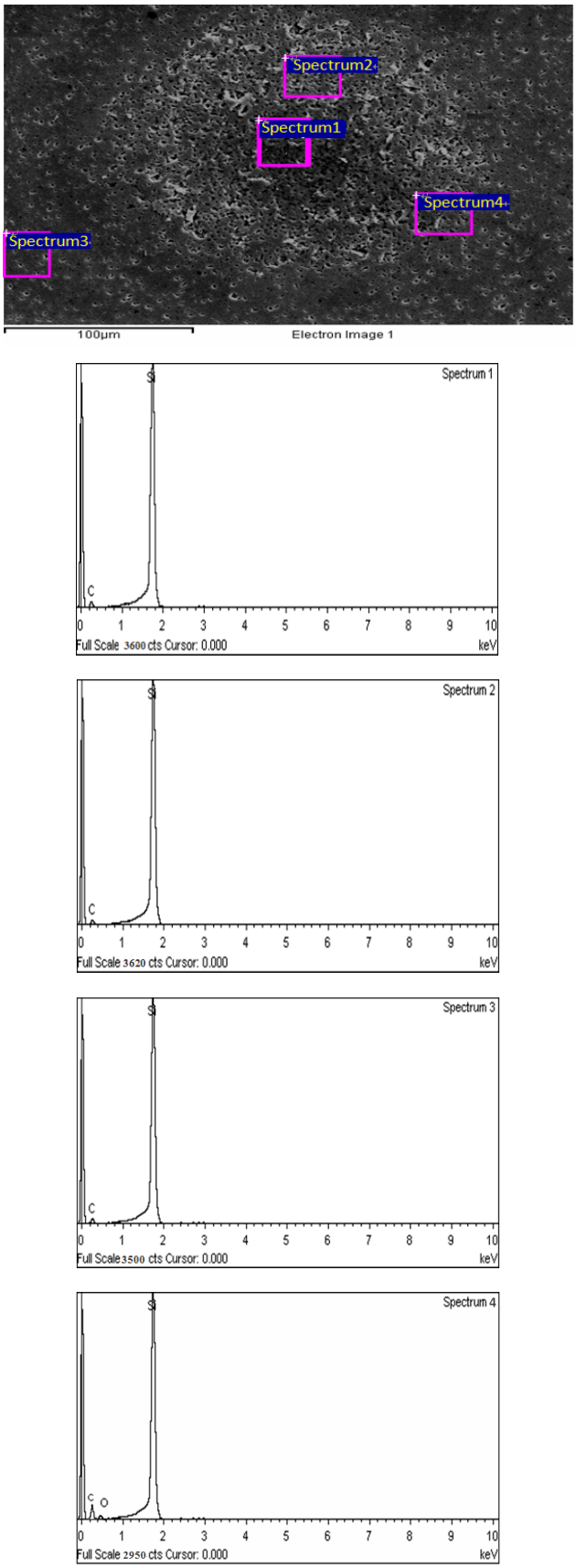

Fig. 10 SEM image and chemical composition of different areas on SiC surface.

5 Conclusions

In this paper, micro-Raman mapping technique was first introduced in the study on the laser ablation mechanisms of SiC ceramics by comparing the composition distributions between unprocessed and laser treated areas. It has been concluded that due to multi-photon absorption, impurity absorption, and photon scattering within SiC, laser energy is accumulated and converted to the heat in the specific region on the SiC surface, causing the ablation in the way of transformation of crystal orientation, decomposition, and oxidation of SiC. It is noticeable that the decomposition of SiC is in the lead in the laser process of SiC ceramics, while the formation of SiO_2 from the oxidation can be only detected in small amount, maybe because of deficiency of O_2 atmosphere in the ablated area, elimination of SiO_2 by carbon at 1505 ℃, or evaporating at 2230 ℃.

Laser ablation on the SiC ceramics is an efficient and accurate surface processing technique by nanosecond or even shorter pulsed laser. For low-absorption and high-LIDT mirrors applied in space optical systems and high-power lasers, it is essential to further optimize the preparation process and the surface modification of SiC ceramics to reduce the material defects and lattice defects, improve the high density, and improve the surface quality.

Acknowledgements

This work is supported by funds from the National Natural Science Foundation of China (NSFC, Contract Nos. 51102266 and 51471182).

References

[1] Jiang F, Liu Y, Yang Y, *et al*. Research progress of optical fabrication and surface-microstructure modification of SiC. *Journal of Nanomaterials* 2012, **2012**: 984048.

[2] Liu G, Huang Z, Liu X, *et al*. Removal behaviors of different SiC ceramics during polishing. *J Mater Sci Technol* 2010, **26**: 125–130.

[3] Yang YT, Ekinci KL, Huang XMH, *et al*. Monocrystalline silicon carbide nanoelectromechanical systems. *Appl Phys Lett* 2001, **78**: 162.

[4] Mehregany M, Zorman CA. SiC MEMS: Opportunities and challenges for applications in harsh environments. *Thin Solid Films* 1999, **355–356**: 518–524.

[5] Mahajan S. Origins of micropipes in SiC crystals. *Appl Phys Lett* 2002, **80**: 4321.

[6] Dong Y, Molian P. Femtosecond pulsed laser ablation of 3C SiC thin film on silicon. *Appl Phys A-Mater* 2003, **77**: 839–846.
[7] Pecholt B, Gupta S, Molian P. Review of laser microscale processing of silicon carbide. *J Laser Appl* 2011, **23**: 012008.
[8] Gupta S, Pecholt B, Molian P. Excimer laser ablation of single crystal 4H-SiC and 6H-SiC wafers. *J Mater Sci* 2011, **46**: 196–206.
[9] Zoppel S, Farsari M, Merz R, *et al*. Laser micro machining of 3C-SiC single crystals. *Microelectron Eng* 2006, **83**: 1400–1402.
[10] Farsari M, Filippidis G, Zoppel S, *et al*. Efficient femtosecond laser micromachining of bulk 3C-SiC. *J Micromech Microeng* 2005, **15**: 1786.
[11] Rudolph P, Brzezinka K-W, Wäsche R, *et al*. Physical chemistry of the femtosecond and nanosecond laser–material interaction with SiC and a SiC–TiC–TiB_2 composite ceramic compound. *Appl Surf Sci* 2003, **208**: 285–291.
[12] Kreutz EW, Weichenhain R, Wagner R, *et al*. Microstructuring of SiC by laser ablation with pulse duration from ns to fs range (LAMP2002). *RIKEN Review* 2003, **2003**: 83–86.
[13] Wasyluk J, Rainey PV, Perova TS, *et al*. Investigation of stress and structural damage in H and He implanted Ge using micro-Raman mapping technique on bevelled samples. *J Raman Spectrosc* 2012, **43**: 448–454.
[14] Burlacov I, Jirkovský J, Müller M, *et al*. Induction plasma-sprayed photocatalytically active titania coatings and their characterisation by micro-Raman spectroscopy. *Surf Coat Technol* 2006, **201**: 255–264.
[15] Nakashima S, Harima H. Raman investigation of SiC polytypes. *phys status solidi a* 1997, **162**: 39–64.
[16] Burton JC, Sun L, Pophristic M, *et al*. Spatial characterization of doped SiC wafers by Raman spectroscopy. *J Appl Phys* 1998, **84**: 6268.
[17] Nakashima S, Kisoda K, Gauthier J-P. Raman determination of structures of long-period SiC polytypes. *J Appl Phys* 1994, **75**: 5354.
[18] Brillante A, Bilotti I, Della Valle RG, *et al*. Characterization of phase purity in organic semiconductors by lattice-phonon confocal Raman mapping: Application to pentacene. *Adv Mater* 2005, **17**: 2549–2553.
[19] Pastorczak M, Wiatrowski M, Kozanecki M, *et al*. Confocal Raman microscopy in 3-dimensional shape and composition determination of heterogeneous systems. *J Mol Struct* 2005, **744–747**: 997–1003.
[20] Furuyama N, Hasegawa S, Hamaura T, *et al*. Evaluation of solid dispersions on a molecular level by the Raman mapping technique. *Int J Pharm* 2008, **361**: 12–18.
[21] Chen J, Huang Z, Chen Z, *et al*. The effect of carbon on surface quality of solid-state-sintered silicon carbide as optical materials. *Mater Charact* 2014, **89**: 7–12.
[22] Alvisi M, De Tomasi F, Perrone MR, *et al*. Laser damage dependence on structural and optical properties of ion-assisted HfO_2 thin films. *Thin Solid Films* 2001, **396**: 44–52.
[23] ISO 11254-1:2000. Lasers and laser-related equipment—Determination of laser-induced damage threshold of optical surfaces—Part 1: 1-on-1 test. 2000.
[24] Wu SG, Tian GL, Xia ZL, *et al*. Influence of negative ion element impurities on laser induced damage threshold of HfO_2 thin film. *Appl Surf Sci* 2006, **253**: 1111–1115.
[25] Xu ZJ. *Detection and Analysis on Semiconductor*, 2nd end. Beijing: Science Press, 2007: 28–194.
[26] Stadelmann R, Hughes B, Orlovskaya N, *et al*. 2D Raman mapping and thermal residual stresses in SiC grains of ZrB_2–SiC ceramic composites. *Ceram Int* 2015, **41**: 13630–13637.
[27] Yu T, Ni Z, Du C, *et al*. Raman mapping investigation of graphene on transparent flexible substrate: The strain effect. *J Phys Chem C* 2008, **112**: 12602–12605.
[28] Goehlert K, Irmer G, Michalowsky L, *et al*. Polytype analysis of SiC powders by Raman spectroscopy. *J Mol Struct* 1990, **219**: 135–140.
[29] Palma C, Rossi MC, Sapia C, *et al*. Laser-induced crystallization of amorphous silicon–carbon alloys studied by Raman microspectroscopy. *Appl Surf Sci* 1999, **138–139**: 24–28.
[30] Veprek S, Sarott F-A, Iqbal Z. Effect of grain boundaries on the Raman spectra, optical absorption, and elastic light scattering in nanometer-sized crystalline silicon. *Phys Rev B* 1987, **36**: 3344.
[31] Yi J, He XD, Sun Y. Characterization of the evaporation behavior of a β-SiC target during electron beam-physical vapor deposition. *J Alloys Compd* 2010, **491**: 436–440.
[32] Yao X-M, Liang H-Q, Liu X-J, *et al*. Effect of carbon source and adding ratio on the microstructure and properties of solid-state sintering silicon carbide. *J Inorg Mater* 2013, **28**: 1009–1013.
[33] Jia TQ, Xu ZZ, Li XX, *et al*. Microscopic mechanisms of ablation and micromachining of dielectrics by using femtosecond lasers. *Appl Phys Lett* 2003, **82**: 4382–4384.
[34] Murahara MM. Excimer-laser-induced photochemical polishing of SiC mirror. In Proceedings of SPIE4679, Laser-Induced Damage in Optical Materials, 2001: 69.
[35] Maekawa M, Kawasuso A, Chen ZQ, *et al*. Structural defects in SiO_2/SiC interface probed by a slow positron beam. *Appl Surf Sci* 2005, **244**: 322–325.
[36] Kurimoto H, Shibata K, Kimura C, *et al*. Thermal oxidation temperature dependence of 4H-SiC MOS interface. *Appl Surf Sci* 2006, **253**: 2416–2420.